We next examined how sensitively YC3.60 reports AP firing in vitro and in vivo by combining targeted electrical recordings with two-photon imaging (see Materials and Methods). Synaptic stimulation of pyramidal neurons in slice cultures elicited single APs or bursts of AP trains as revealed by juxtacellular recordings (Figure 4A). Single APs evoked Ca^{2+} transients with an average $\Delta R/R$ amplitude of 5.9 ± 0.3% (mean ± S.E.M., n = 32), while high-frequency bursts of 2, 3, and 5 APs elicited successively larger transients (10.1 ± 0.3% (40), 13.8 ± 0.4% (35) and 18.7 ± 1.1% (4), respectively). The increase in Ca^{2+} transient amplitude with number of APs was well approximated by a linear fit (Figure 4C; slope = 3.15%/AP; r^2 = 0.98). The decay of Ca^{2+} transients was relatively fast and did not significantly depend on AP number (Figure 4D; time constants of exponential fits: 0.78 ± 0.05 s, 0.82 ± 0.03 s, 0.91 ± 0.04 s, and 0.80 ± 0.06 s for 1, 2, 3 and 5 APs, respectively; slope of linear regression 4 ms/AP).

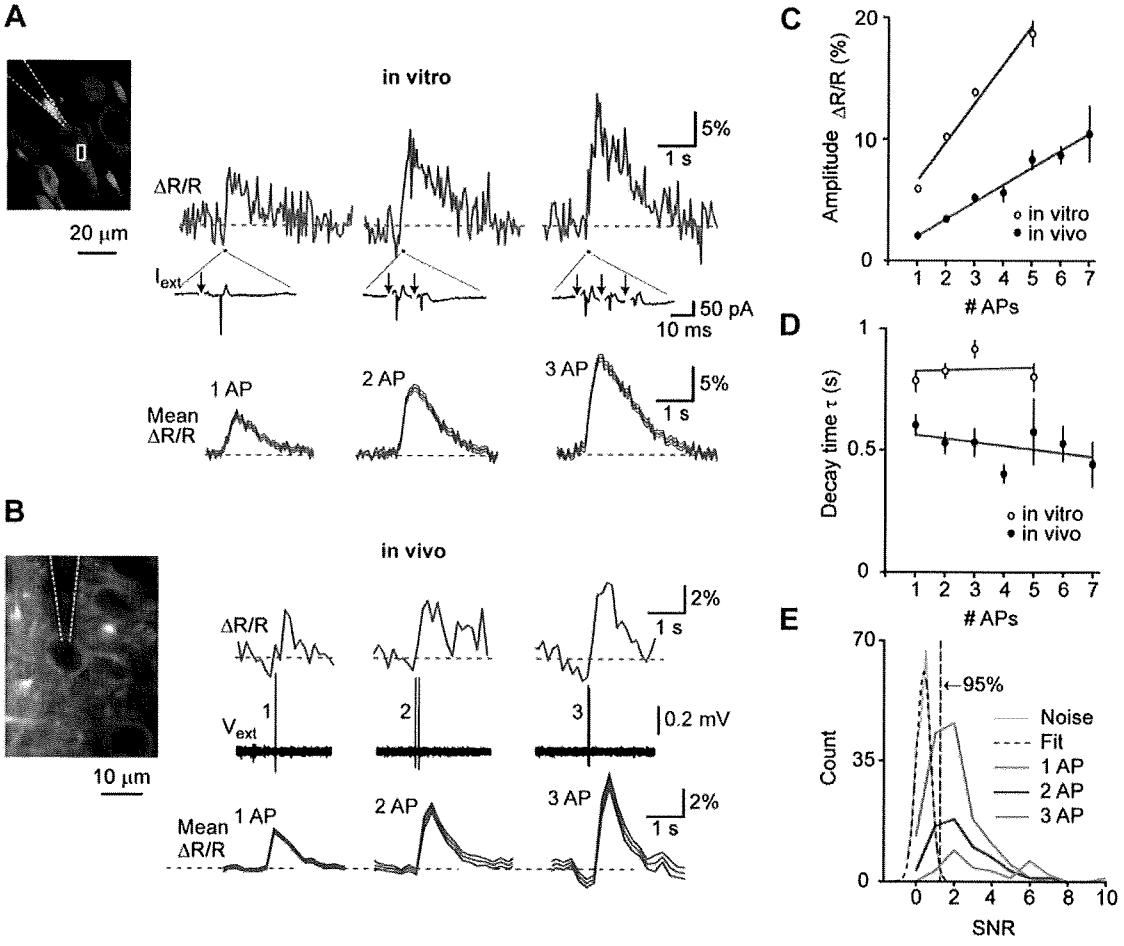

Figure 4. YC3.60 sensitivity to action potentials in vitro and in vivo
(A) Characterization of YC3.60 sensitivity in vitro. Top: Cell-attached recording at room temperature from a hippocampal CA3 pyramidal neuron (left image with recording pipette) and simultaneous fluorescence measurement from a somatic region of interest (white box). Extracellular current and single-trial Ca^{2+} transients are shown in response to 1, 2 and 3 APs elicited by synaptic stimulation (arrows; stimulation pipette not shown;

stimulus artifacts blanked). Bottom: Mean fluorescence traces (±S.E.M.) in response to 1, 2 and 3 APs (n = 32 traces from 4 cells for 1 AP; n = 40 (5) for 2 APs; n = 35 (5) for 3 APs). **(B)** Characterization of YC3.60 sensitivity in vivo. Top: Juxtacellular voltage recording from a L2/3 neuron in barrel cortex (left image with recording pipette) and simultaneous two-photon Ca^{2+} measurement from the soma region. Example Ca^{2+} transients are shown for spontaneously occurring 1, 2 and 3 APs. Bottom: Mean fluorescence traces (±S.E.M.) in response to 1, 2 and 3 APs (n = 78 traces from 9 cells for 1 AP; n = 33 (7) for 2 APs; n = 23 (7) for 3 APs). **(C)** Peak amplitudes of Ca^{2+} transients as a function of number of APs (in vitro, open circles, n = 32, 40, 35 and 4 transients for 1, 2, 3 and 5 APs, respectively; in vivo, filled circles, n = 138 transients from 11 cells, 61 (9), 30 (9), 18 (7), 12 (6), 4 (3), 6 (5) for 1-7 APs, respectively). **(D)** Decay time constants of exponential fits as a function of number of APs (in vitro, open circles, same n as in C; in vivo, filled circles n =78 (9), 33 (7), 23 (7), 16 (6), 11 (5), 3 (2), 5 (5) for 1-7 APs, respectively). Red lines are linear regressions. Error bars are shown as S.E.M. **(E)** Efficiency of AP detection in vivo was determined by estimating the distribution of the signal to noise ratio (SNR) under noise conditions (solid blue) and fitting with a Gaussian (broken blue). From the fit, we determined the SNR cutoff at which less than 5% of baseline traces would be classified as false positives (SNR = 1.3). Using this threshold, 71% of single APs (97 / 137), 80% of doublets (48 / 60) and 93% of triplets (27 / 29) were correctly detected.

To determine YC3.60 sensitivity in vivo, we performed two-photon targeted juxtacellular recordings from YC3.60-expressing L2/3 neurons in barrel cortex of anesthetized mice (Figure 4B). In many cases, single APs were associated with clear ΔR/R transients. On average, single APs elicited transients of 2.00 ± 0.09% peak amplitude (n = 138 transients from 11 cells). Bursts of up to 7 APs elicited transients with successively larger amplitude (Figure 4C). The relationship between Ca^{2+} transient amplitude and AP number again was well approximated by a linear fit (slope = 1.39%/AP; r^2 = 0.98), indicating that YC3.60 fluorescence changes for bursts of APs were well below saturation. Indeed, much larger events (20–30% ΔR/R) were occasionally observed in response to trains of 10 or more APs (see Figure 5B). We estimated AP-detection efficiency by comparing the signal-to-noise ratio of AP-evoked transients to the baseline noise level (see Materials and Methods). Detection rates were 71% for single APs and 80% and 93% for bursts of 2 and 3 APs, respectively (Figure 4E). Similar to the in vitro results, Ca^{2+} transients showed fast decays, which did not depend on AP number (Figure 4D; for single APs 0.60 ± 0.05 s; n = 78 transients from 9 cells; slope of linear regression -16 ms/AP). The differences in absolute values for peak amplitudes and decay time constants between in vitro and in vivo experiments most likely can be attributed to the differences in experimental conditions. In particular, a similar reduction of AP-evoked Ca^{2+} transient amplitude at physiological compared to room temperature has also been reported for other FCIPs (Mao et al., 2008; Tian et al., 2009). We conclude that YC3.60 sensitively reports AP firing both in vitro and in vivo and that it can even resolve single APs.

3.3. Sensory-evoked and spontaneous subcellular, cellular and wide-field Ca^{2+} signals

We next investigated in how far YC3.60 can be used to study sensory-evoked cortical activity on various spatial scales, ranging from dendrites of individual neurons to large areas of the barrel field. On the finest scale, we simultaneously measured spontaneous dendritic and somatic Ca^{2+} transients in L2/3 pyramidal neurons using 'arbitrary plane' imaging (Göbel and Helmchen, 2007b) (Figure 5A). As expected (Schiller et al., 1995), Ca^{2+} transients showed faster decay times in apical dendrites compared to somata (0.35 ± 0.04 s vs. 0.47 ± 0.04 ms; $n = 23$; $p < 0.01$; paired 2-tailed t-test), confirming relatively rapid kinetics of YC3.60. A large dynamic range of YC3.60 is demonstrated in Figure 5B, where Ca^{2+} transients evoked by complex AP patterns (ranging from individual APs to trains of 10 or more APs) were revealed with high fidelity. The peak ΔR/R amplitudes of around 30% in these recordings presumably still are far from indicator saturation (see Figure 3A).

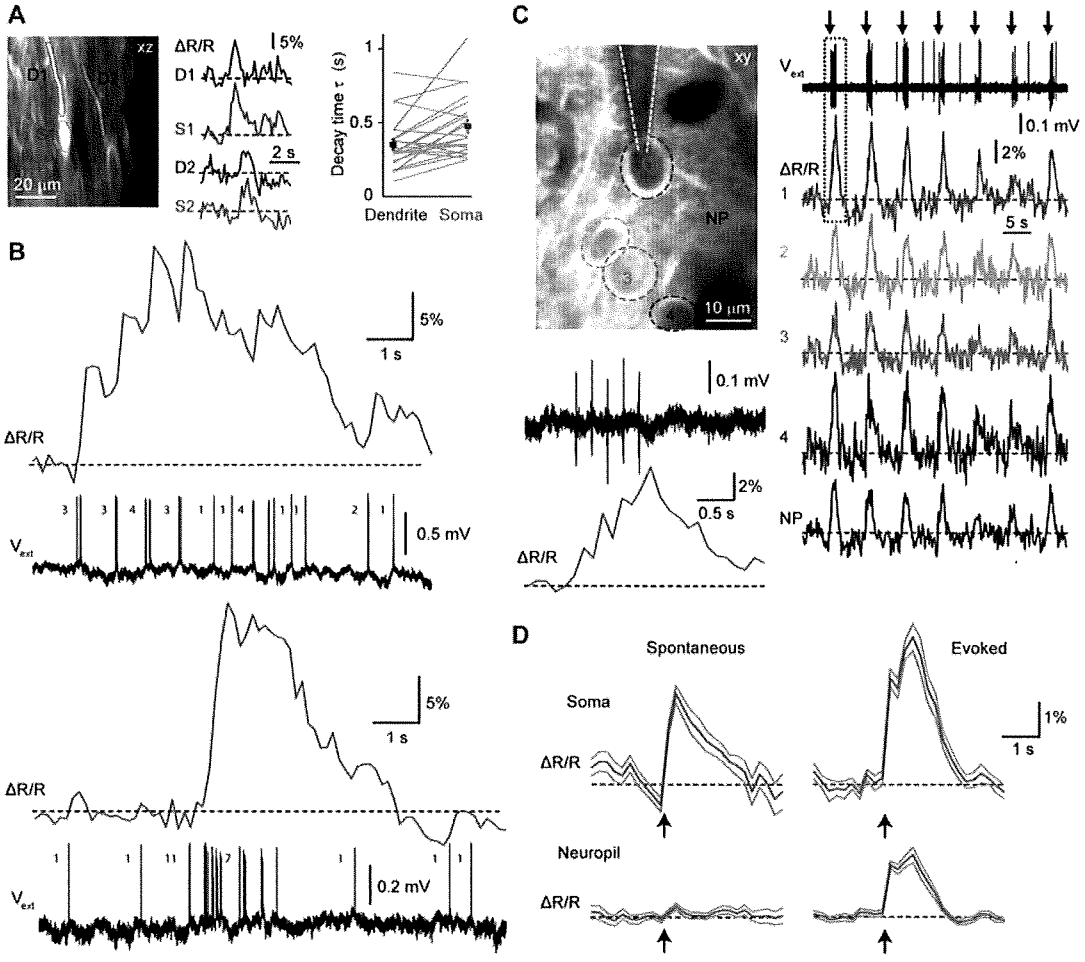

Figure 5. Single-cell and population YC3.60 Ca^{2+} signals in L2/3 of barrel cortex
(A) Simultaneous two-photon Ca^{2+} imaging in soma and dendrites of L2/3 neurons using vertical (xz-)imaging. Examples of spontaneous somatic (S, red) and apical dendritic (D, blue) YC3.60 Ca^{2+} transients for the cells depicted in the left image. Right: Mean decay times in dendrites compared to somata for 23 measurements (grey lines; mean±S.E.M).

(B) Simultaneous juxtacellular voltage recording and two-photon Ca^{2+} imaging from a neuron showing rare events of sustained and high-frequency AP firing in L2/3 neurons that are accompanied by large YC3.60 Ca^{2+} transients with peak amplitudes of up to 30% ΔR/R. Top: Sustained AP firing leads to prolonged elevation of the fluorescence ratio. Bottom: A short burst of 11 APs is accompanied by a fast Ca^{2+} transient, which returns to baseline following a stereotypical exponential decay. **(C)** Two-photon Ca^{2+} imaging of a small population of neurons during sensory stimulation (seven times 5 air-puffs to contra-lateral whiskers at 5 Hz). Large Ca^{2+} transients in cell 1 (red trace) correlated with the spiking activity observed in the simultaneous juxtacellular voltage recording. Concomitant Ca^{2+} transients were also evoked in neighboring neuronal somata and in the nearby neuropil (NP). The response to the first stimulation episode (dashed box) is shown on expanded scale in the lower left, indicating that YC3.60 resolves the individual steps in the accumulated Ca^{2+} response. **(D)** Event-triggered average Ca^{2+} traces from somata and adjacent neuropil for spontaneous (n = 37 events of 1–3 APs) and evoked (n = 32 events of 1–5 APs) action potentials. Multi-whisker air puff-evoked Ca^{2+} transients in somata were significantly larger than those in the neuropil while spontaneous spikes were accompanied by somatic but no neuropil transients. Errors are shown as S.E.M.

On the level of local neuronal populations, air-puff whisker stimulation (5 Hz) elicited clear Ca^{2+} transients in neuronal somata but also in the neuropil (Figure 5C). Bursts of AP firing could be distinguished even at relatively slow frame rates (7.81 Hz), highlighting the rapid kinetics of the Ca^{2+} sensor. Combined electrical recordings allowed to directly assess the degree of potential contamination of somatic signals by Ca^{2+} signals in the surrounding neuropil (Göbel and Helmchen, 2007a; Kerr et al., 2005). Whisker-evoked events were associated with significantly larger Ca^{2+} transients in somata compared to the neighboring neuropil (4.0 ± 0.5 vs. 1.6 ± 0.2% ΔR/R, $n = 32$, $p < 0.01$, paired 2-tailed t-test). In contrast, spontaneously occurring APs elicited Ca^{2+} transients in somata but not in the neuropil (2.3 ± 0.4% vs. 0.4 ± 0.1%, $n = 37$, $p < 0.01$). (Figure 5D-E). From these observations we conclude that sensory stimulation can evoke Ca^{2+} transients in the neuropil in addition to somatic signals, presumably reflecting excitation of afferent axonal pathways (Kerr et al., 2005), but that high-resolution two-photon imaging clearly distinguishes the cellular AP-evoked signals.

Activation of a substantial fraction of neurons in the local population as well as of the surrounding neuropil might cause sufficient YC3.60 signals for large-scale bulk recording of barrel cortex excitation. Indeed, in addition to sensory-evoked responses spontaneous fluctuating calcium signals were apparent in the neuropil when entire two-photon imaging frames were used as ROI (Figure 6A). Similar spontaneous YC3.60 signals were observed with wide-field single-photon-excited fluorescence with a CCD-camera positioned above barrel cortex (Figure 6B). These slow oscillations closely corresponded to the simultaneously measured local field potential (LFP) and most likely are due to synchronous activity during anesthesia. In addition, air puff stimulation of whiskers evoked stimulus-locked LFP signals and bulk fluorescence changes with an average $\Delta F/F_{YFP}$ amplitude of 0.47±0.03% and an average decay time of 0.48±0.04 s ($n = 3$ animals). Bulk-activity in barrel cortex could also be read out using single-photon excitation and fluorescence collection through a single-core optical fiber (440 μm core

diameter; see Material and Methods). With the optical fiber placed on top of the dura (or the thinned skull) of anesthetized mice showing YC3.60 expression in barrel cortex, we observed both spontaneous and air puff-evoked $\Delta F/F_{YFP}$ signals (Figure 6C) that were similar to the signals observed by wide-field camera imaging.

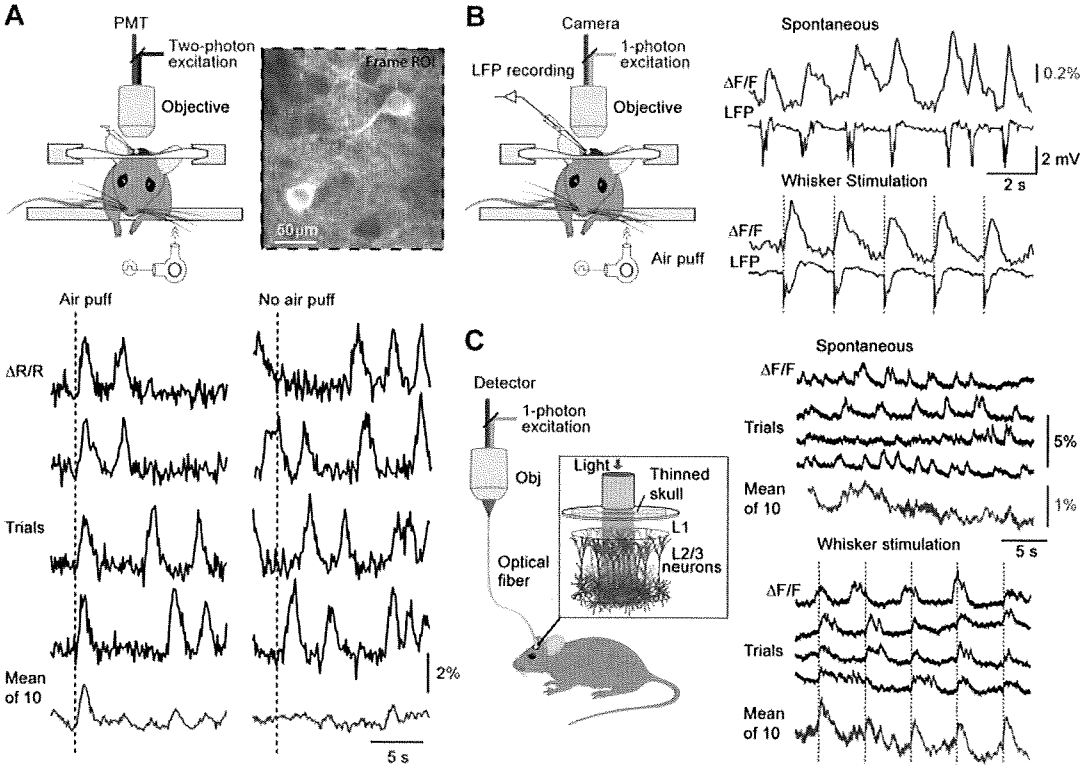

Figure 6. Bulk recording of spontaneous and sensory-evoked YC3.60 Ca^{2+} signals in barrel cortex

(A) Large-area Ca^{2+} imaging using two-photon excitation and whisker stimulation by air puffs. Neuropil and two neurons visible about 100 µm deep in a 12-week-old mouse ~6 weeks after virus infection. The entire frame was taken as region of interest. Bottom: Examples of single-trial spontaneous and sensory-evoked responses are shown along with average traces of 10 trials. **(B)** Large-area Ca^{2+} imaging using single-photon excitation and a camera and simultaneous local-field potential recording (LFP) in barrel cortex of an anesthetized mouse (left schematic). Right: The mean YC3.60 fluorescence signal (ΔF/F in YFP-channel; red traces) correlated well with the LFP for both spontaneous activity (top) and upon air-puff whisker stimulation (bottom; dashed vertical lines). **(C)** Fiber-optic bulk recording of YC3.60 signals in barrel cortex in an anesthetized mouse (left schematic). Fluorescence excitation and detection were both accomplished through the optical fiber, the tip of which was placed on the cortical surface. Right: Examples of single-trial YC3.60 fluorescence traces (ΔF/F in YFP-channel) and mean of 10 traces for spontaneous activity (top) and upon air-puff whisker stimulation (bottom; dashed vertical lines).

3.4. Fiber-optic recording of barrel cortex activity in freely moving mice

Fiber-optic recordings enable measurements of neuronal activity in awake, freely behaving animals (Adelsberger et al., 2005; Murayama and Larkum, 2009b; Murayama et al., 2007; for review see Grewe and Helmchen, 2009; Wilt et al., 2009). We tested if YC3.60 expression is suitable for such an application. Using firm attachment of the single optical fiber to the animal's head (Murayama and Larkum, 2009b) we measured bulk fluorescence from the barrel field in awake, freely moving mice (Figure 7). While the mice were either passively sitting or actively exploring, we recorded complex $\Delta F/F_{YFP}$ signals (Figure 7A-C). We could block the Ca^{2+} transients by application of Cd^{2+}, a Ca^{2+} channel blocker, to the cortical surface (Figure 7D), indicating that the YC3.60 sensor was reporting Ca^{2+} transients. Mechanically jolting the fiber did not result in obvious fluorescence changes in YC3.60-expressing mice as in previous fiber-optic studies (Murayama and Larkum, 2009b; Murayama et al., 2007). Furthermore, fluorescence traces in a wild-type mouse (without YC3.60) were flat without any movement-related changes (Figure 7E). Together these findings exclude opto-mechanical artifacts as source of the observed fluorescence changes and instead indicate that YC3.60 signals are caused by Ca^{2+} channel activation and thus provide a readout of the complex activation pattern in the barrel cortex. Fiber-optic recordings using YC3.60 thus should permit closer investigation of behavioral-related activity in specific neocortical areas.

4. Discussion

In vivo Ca^{2+} imaging in the mammalian neocortex so far mainly relied on synthetic indicator dyes (Garaschuk et al., 2006; Gobel and Helmchen, 2007a; Grewe and Helmchen, 2009; Kerr and Denk, 2008). Recently, different FCIPs (also called genetically encoded Ca^{2+} indicators or GECIs) have been developed that will allow for a more specific interrogation of various aspects of neural activity, compared to synthetic sensors. Here, we have shown that upon neuron-specific expression in the mouse neocortex, the FCIP, YC3.60, can be used to read out activation of neocortical areas at different spatial scales both in anaesthetized and awake, freely moving animals.

Original characterization of YC3.60 (Nagai et al., 2004) defined it as an indicator with high sensitivity and dynamic range in vitro. However, reliable Ca^{2+} imaging in vivo was not demonstrated in transgenic animals (Nagai et al., 2004), possibly due to the use of a plasma-membrane bound version of the sensor which may have resulted in a reduced AP detection efficiency (Mao et al., 2008). Subsequently, YC3.60 was employed to obtain quantitative Ca^{2+} concentration measurements in brain slices (Liu et al., 2008) and resting Ca^{2+} concentrations in vivo (Kuchibhotla et al., 2008). The current study extends these findings by demonstrating that viral delivery of YC3.60 permits in vivo measurements of sensory-evoked Ca^{2+} signals that closely correspond to cellular AP firing patterns. Furthermore, we have shown that YC3.60 can be applied to monitor neural activity at diverse spatial scales, covering dendritic Ca^{2+} signals, AP firing in local neuronal populations as well as large scale brain areas.

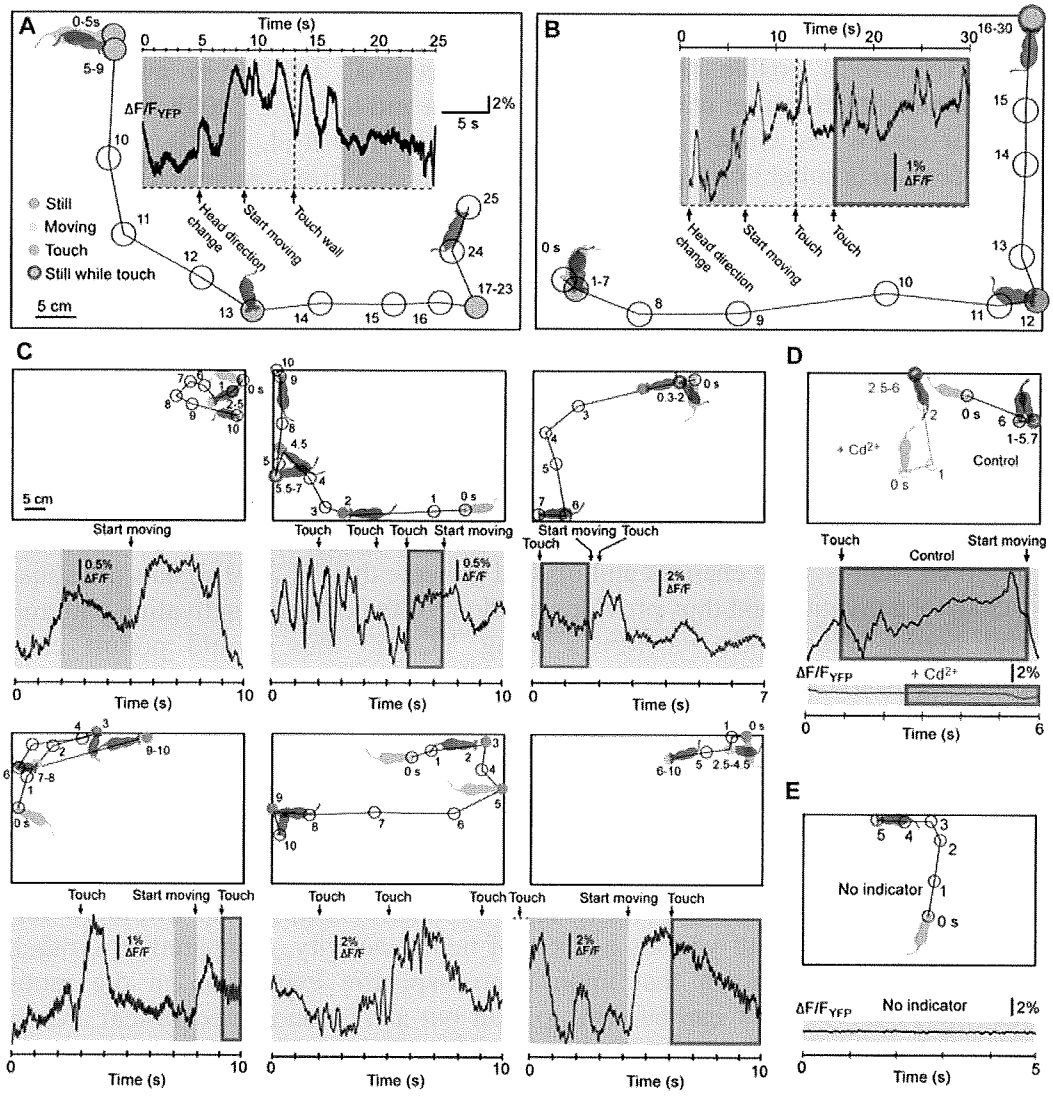

Figure 7. Fiber-optic recording of brain area activity in freely moving mice using YC3.60.

(A and B) Two examples of fiber-optic recording of YC3.60 signals in awake, freely moving mice. Bulk Ca^{2+} signals indicating neuronal activity were recorded in somatosensory cortex through a single-core optical fiber as shown in Fig. 6C. Fluorescence changes in the YFP-channel are shown during 25-30 s periods together with the position of the mouse in an open field box. Animal behavior (sitting still, moving, touches, or having contact to the wall) is indicated by background colors. The trajectory of the animals' movement is indicated with selected time stamps. **(C)** Six more examples of Ca^{2+} imaging from 3 mice, together with corresponding behavioral observations. Changes of the animal's behavioral state (e.g. start of movement) were frequently associated with marked discontinuities in the fluorescence trace, indicating complex underlying Ca^{2+} dynamics. **(D)** Control experiment showing that Ca^{2+} signals are blocked by local perfusion of the cortical region with Cd^{2+}. **(E)** Control experiment demonstrating that a flat fluorescence trace is observed in the absence of YC3.60 expression.

Gene delivery by AAV-vectors (Zhu et al., 2007) provides a highly flexible, straightforward and safe approach for dense and wide-spread expression of FCIPs in neurons (Kootstra and Verma, 2003). For these reasons, viral delivery has been the method of choice in recent characterizations of FCIPs in the mammalian brain (Mank et al., 2008; Tian et al., 2009; Wallace et al., 2008). An alternative approach for gene delivery of FCIPs into the brain is in utero electroporation, which provides the potential benefit of cell-type specificity, depending on the precise electroporation protocol (Borrell et al., 2005) but which results in relatively sparse labeling of neurons compared to viral delivery (Mank et al., 2008). Finally, the production of transgenic mice expressing a number of different FCIPs has been reported (Hasan et al., 2004; Heim et al., 2007) including membrane-bound YC3.60 (Nagai et al., 2004). In one of these studies, sensory-evoked Ca^{2+} transients were demonstrated using wide-field imaging of the olfactory bulb with two FCIPs expressed under a tetracycline-inducible promoter (Hasan et al., 2004). The widespread use of these mouse lines has been limited, however, by the failure to clearly monitor AP-evoked cellular Ca^{2+} signals in vivo, possibly due to low protein expression levels.

Comprehensive analysis of neural circuits will require reliable detection of single APs as well as estimation of the firing frequency during bursts of APs. Here we demonstrate that YC3.60 can detect the occurrence of single APs in pyramidal cells of mouse barrel cortex in vivo with a sensitivity comparable to recent reports of another ratiometric FCIP, D3cpV (Wallace et al., 2008). Unlike D3cpV, however, YC3.60 shows faster kinetics and minimal saturation for bursts of up to at least 10 APs, thus making it a suitable tool for quantitative investigation of local neural network dynamics in vivo. Overall our analysis revealed that YC3.60 shows comparable signals in terms of sensitivity and decay times to the commonly used synthetic indicator Oregon Green BAPTA-1 (Kerr et al., 2005), which has been used extensively for optical monitoring of AP firing in populations of neurons. Recently, in addition to D3cpV, two other novel FCIPs have been proposed for in vivo two-photon Ca^{2+} imaging in the mammalian brain. First, in utero electroporation of TN-XXL, a troponin-based ratiometric FCIP, allowed repeated Ca^{2+} imaging from the same neurons over days; however its sensitivity to AP firing was relatively low with single AP detection only achievable in brain slices (Mank et al., 2008). Second, AAV-delivery of the single-fluorescent protein sensor GCaMP-3 has recently been shown to exhibit large fluorescence changes and to detect APs with fast kinetics and little saturation in mouse somatosensory cortex in vivo (Tian et al., 2009). This Ca^{2+} sensor does not, however, permit ratiometric imaging and thus will be more susceptible to motion artifacts compared to YC3.60. It is likely that in the near future improved versions of either cameleons or GCaMPs will provide even better optical readout of neuronal spiking. Furthermore, single-fluorophore FCIPs may be co-expressed with a second indicator that is not Ca^{2+}-sensitive in order to reduce their susceptibility to motion artifacts.

In addition to two-photon Ca^{2+} imaging at the level of single cells and small populations of neurons, we demonstrated the use of FCIPs to record large-scale neuronal activity in awake, freely moving animals. Using a fiber-optic approach (Murayama and Larkum, 2009b; Murayama et al., 2007) to image bulk neural activity in mouse barrel cortex, we

showed complex Ca^{2+} dynamics associated with behaviorally salient events such as object-touching or moving. We suggest that these activity patterns may reflect the dynamic interaction of different behavior-related brain states with sensory-evoked activity.

In conclusion, viral delivery of YC3.60 provides a powerful tool for the optical interrogation of neural circuits at multiple spatial scales and with high sensitivity. Viral delivery of FCIPs may in the future be combined with the powerful tools of mouse genetics, allowing for cell-type specific or inducible expression of Ca^{2+} sensors (Wallace et al., 2008; Zhu et al., 2007). Thus, injection of AAV-FCIP vectors with loxP sites (Atasoy et al., 2008; Kuhlman and Huang, 2008) into Cre driver mouse lines should allow selective expression of YC3.60 in specific cortical layers (Madisen et al.) and interneuron subtypes (Chattopadhyaya et al., 2004; Oliva et al., 2000). Cell-type specific expression, combined with fiber optic recordings in freely moving animals, will allow functional correlation of specific neuronal populations with behavior. Moreover, the approach developed here may conceivably be adapted to other mammalian species, such as rats (Foti et al., 2007) or even non-human primates (Stettler et al., 2006) and is therefore likely to play an important role in the dissection of the neural underpinnings of complex behaviors.

Acknowledgments

We like to thank Winfried Denk and Peter H. Seeburg for generous support and interest in the project, and Andreas Schaefer for supporting T.H. We also thank Erika Heil for art work (Art for Biomed, Frankfurt, Germany) and Matthias Heindorf for help on plots. This work was supported by the Max Planck Society, Collaborative Research Grant (SFB636/A4), Volkswagen foundation (AZ: I/80 704) to R.S., a grant from the Swiss National Science Foundation (#3100A0-114624) to F.H., a grant from the Swiss Systems Biology Initiative SystemsX.ch to F.H. and M.L. (Neurochoice project), the German Academic Exchange Service (DAAD) to H.L., the Sumitomo Foundation and Research Foundation for Opto-Science and Technology to M.M., and Schloessmann Foundation and Fritz Thyssen Stiftung to M.T.H.

References

Adelsberger, H., Garaschuk, O., and Konnerth, A. (2005). Cortical calcium waves in resting newborn mice. Nat Neurosci *8*, 988-990.

Atasoy, D., Aponte, Y., Su, H.H., and Sternson, S.M. (2008). A FLEX switch targets Channelrhodopsin-2 to multiple cell types for imaging and long-range circuit mapping. J Neurosci *28*, 7025-7030.

Berger, T., Borgdorff, A., Crochet, S., Neubauer, F.B., Lefort, S., Fauvet, B., Ferezou, I., Carleton, A., Lüscher, H.R., and Petersen, C.C. (2007). Combined voltage and calcium epifluorescence imaging in vitro and in vivo reveals subthreshold and suprathreshold dynamics of mouse barrel cortex. J Neurophysiol *97*, 3751-3762.

Borrell, V., Yoshimura, Y., and Callaway, E.M. (2005). Targeted gene delivery to telencephalic inhibitory neurons by directional in utero electroporation. J Neurosci Methods *143*, 151-158.

Chattopadhyaya, B., Di Cristo, G., Higashiyama, H., Knott, G.W., Kuhlman, S.J., Welker, E., and Huang, Z.J. (2004). Experience and activity-dependent maturation of perisomatic GABAergic innervation in primary visual cortex during a postnatal critical period. J Neurosci *24*, 9598-9611.

Foti, S., Haberman, R.P., Samulski, R.J., and McCown, T.J. (2007). Adeno-associated virus-mediated expression and constitutive secretion of NPY or NPY13-36 suppresses seizure activity in vivo. Gene therapy *14*, 1534-1536.

Garaschuk, O., Milos, R.I., and Konnerth, A. (2006). Targeted bulk-loading of fluorescent indicators for two-photon brain imaging in vivo. Nat Protoc *1*, 380-386.

Göbel, W., and Helmchen, F. (2007a). In vivo calcium imaging of neural network function. Physiology (Bethesda) *22*, 358-365.

Göbel, W., and Helmchen, F. (2007b). New angles on neuronal dendrites in vivo. J Neurophysiol *98*, 3770-3779.

Grewe, B.F., and Helmchen, F. (2009). Optical probing of neuronal ensemble activity. Curr Opin Neurobiol.

Hasan, M.T., Friedrich, R.W., Euler, T., Larkum, M.E., Giese, G., Both, M., Duebel, J., Waters, J., Bujard, H., Griesbeck, O., *et al.* (2004). Functional fluorescent Ca^{2+} indicator proteins in transgenic mice under TET control. PLoS Biol *2*, e163.

Heim, N., Garaschuk, O., Friedrich, M.W., Mank, M., Milos, R.I., Kovalchuk, Y., Konnerth, A., and Griesbeck, O. (2007). Improved calcium imaging in transgenic mice expressing a troponin C-based biosensor. Nat Methods *4*, 127-129.

Helmchen, F., and Denk, W. (2005). Deep tissue two-photon microscopy. Nat Methods *2*, 932-940.

Helmchen, F., Imoto, K., and Sakmann, B. (1996). Ca^{2+} buffering and action potential-evoked Ca^{2+} signaling in dendrites of pyramidal neurons. Biophys J *70*, 1069-1081.

Helmchen, F., Svoboda, K., Denk, W., and Tank, D.W. (1999). In vivo dendritic calcium dynamics in deep-layer cortical pyramidal neurons. Nat Neurosci *2*, 989-996.

Hires, S.A., Tian, L., and Looger, L.L. (2008). Reporting neural activity with genetically encoded calcium indicators. Brain Cell Biol *36*, 69-86.

Kerr, J.N., de Kock, C.P., Greenberg, D.S., Bruno, R.M., Sakmann, B., and Helmchen, F. (2007). Spatial organization of neuronal population responses in layer 2/3 of rat barrel cortex. J Neurosci *27*, 13316-13328.

Kerr, J.N., and Denk, W. (2008). Imaging in vivo: watching the brain in action. Nat Rev Neurosci *9*, 195-205.

Kerr, J.N., Greenberg, D., and Helmchen, F. (2005). Imaging input and output of neocortical networks in vivo. Proc Natl Acad Sci U S A *102*, 14063-14068.

Kootstra, N.A., and Verma, I.M. (2003). Gene therapy with viral vectors. Annu Rev Pharmacol Toxicol *43*, 413-439.

Kuchibhotla, K.V., Goldman, S.T., Lattarulo, C.R., Wu, H.-Y., Hyman, B.T., and Bacskai, B.J. (2008). Abeta plaques lead to aberrant regulation of calcium homeostasis in vivo resulting in structural and functional disruption of neuronal networks. Neuron *59*, 214-225.

Kügler, S., Hahnewald, R., Garrido, M., and Reiss, J. (2007). Long-term rescue of a lethal inherited disease by adeno-associated virus-mediated gene transfer in a mouse model of molybdenum-cofactor deficiency. Am J Hum Genet *80*, 291-297.

Kuhlman, S.J., and Huang, Z.J. (2008). High-resolution labeling and functional manipulation of specific neuron types in mouse brain by Cre-activated viral gene expression. PloS one *3*, e2005.

Liu, X., Gong, H., Li, X., and Zhou, W. (2008). Monitoring calcium concentration in neurons with cameleon. J Biosci Bioeng *105*, 106-109.

Madisen, L., Zwingman, T.A., Sunkin, S.M., Oh, S.W., Zariwala, H.A., Gu, H., Ng, L.L., Palmiter, R.D., Hawrylycz, M.J., Jones, A.R., *et al.* A robust and high-throughput Cre reporting and characterization system for the whole mouse brain. Nat Neurosci *13*, 133-140.

Mank, M., and Griesbeck, O. (2008). Genetically encoded calcium indicators. Chem Rev *108*, 1550-1564.

Mank, M., Santos, A.F., Direnberger, S., Mrsic-Flogel, T.D., Hofer, S.B., Stein, V., Hendel, T., Reiff, D.F., Levelt, C., Borst, A., *et al.* (2008). A genetically encoded calcium indicator for chronic in vivo two-photon imaging. Nat Methods *5*, 805-811.

Mao, T., O'Connor, D.H., Scheuss, V., Nakai, J., and Svoboda, K. (2008). Characterization and subcellular targeting of GCaMP-type genetically-encoded calcium indicators. PLoS ONE *3*, e1796.

Markram, H., and Sakmann, B. (1994). Calcium transients in dendrites of neocortical neurons evoked by single subthreshold excitatory postsynaptic potentials via low-voltage-activated calcium channels. Proc Natl Acad Sci U S A *91*, 5207-5211.

Mastakov, M.Y., Baer, K., Xu, R., Fitzsimons, H., and During, M.J. (2001). Combined injection of rAAV with mannitol enhances gene expression in the rat brain. Mol Ther *3*, 225-232.

Miyawaki, A., Llopis, J., Heim, R., McCaffery, J.M., Adams, J.A., Ikura, M., and Tsien, R.Y. (1997). Fluorescent indicators for Ca^{2+} based on green fluorescent proteins and calmodulin. Nature *388*, 882-887.

Miyawaki, A., Nagai, T., and Mizuno, H. (2005). Engineering fluorescent proteins. Adv Biochem Eng Biotechnol *95*, 1-15.

Murayama, M., and Larkum, M.E. (2009a). Enhanced dendritic activity in awake rats. Proc Natl Acad Sci U S A *106*, 20482-20486.

Murayama, M., and Larkum, M.E. (2009b). In vivo dendritic calcium imaging with a fiberoptic periscope system. Nat Protoc *4*, 1551-1559.

Murayama, M., Perez-Garci, E., Lüscher, H.R., and Larkum, M.E. (2007). Fiberoptic system for recording dendritic calcium signals in layer 5 neocortical pyramidal cells in freely moving rats. J Neurophysiol *98*, 1791-1805.

Murayama, M., Perez-Garci, E., Nevian, T., Bock, T., Senn, W., and Larkum, M.E. (2009). Dendritic encoding of sensory stimuli controlled by deep cortical interneurons. Nature *457*, 1137-1141.

Nagai, T., Yamada, S., Tominaga, T., Ichikawa, M., and Miyawaki, A. (2004). Expanded dynamic range of fluorescent indicators for Ca^{2+} by circularly permuted yellow fluorescent proteins. Proc Natl Acad Sci U S A *101*, 10554-10559.

Nimmerjahn, A., Kirchhoff, F., Kerr, J.N., and Helmchen, F. (2004). Sulforhodamine 101 as a specific marker of astroglia in the neocortex in vivo. Nat Methods *1*, 31-37.

Oliva, A.A., Jr., Jiang, M., Lam, T., Smith, K.L., and Swann, J.W. (2000). Novel hippocampal interneuronal subtypes identified using transgenic mice that express green fluorescent protein in GABAergic interneurons. J Neurosci *20*, 3354-3368.

Palmer, A.E., Giacomello, M., Kortemme, T., Hires, S.A., Lev-Ram, V., Baker, D., and Tsien, R.Y. (2006). Ca^{2+} indicators based on computationally redesigned calmodulin-peptide pairs. Chem Biol *13*, 521-530.

Palmer, A.E., and Tsien, R.Y. (2006). Measuring calcium signaling using genetically targetable fluorescent indicators. Nat Protoc *1*, 1057-1065.

Sato, T.R., Gray, N.W., Mainen, Z.F., and Svoboda, K. (2007). The Functional Microarchitecture of the Mouse Barrel Cortex. PLoS Biol *5*, e189.

Schiller, J., Helmchen, F., and Sakmann, B. (1995). Spatial profile of dendritic calcium transients evoked by action potentials in rat neocortical pyramidal neurones. J Physiol *487 (Pt 3)*, 583-600.

Stettler, D.D., Yamahachi, H., Li, W., Denk, W., and Gilbert, C.D. (2006). Axons and synaptic boutons are highly dynamic in adult visual cortex. Neuron *49*, 877-887.

Stoppini, L., Buchs, P.A., and Muller, D. (1991). A simple method for organotypic cultures of nervous tissue. J Neurosci Methods *37*, 173-182.

Stosiek, C., Garaschuk, O., Holthoff, K., and Konnerth, A. (2003). In vivo two-photon calcium imaging of neuronal networks. Proc Natl Acad Sci U S A *100*, 7319-7324.

Svoboda, K., Denk, W., Kleinfeld, D., and Tank, D.W. (1997). In vivo dendritic calcium dynamics in neocortical pyramidal neurons. Nature *385*, 161-165.

Tian, L., Hires, S.A., Mao, T., Huber, D., Chiappe, M.E., Chalasani, S.H., Petreanu, L., Akerboom, J., McKinney, S.A., Schreiter, E.R., *et al.* (2009). Imaging neural activity in worms, flies and mice with improved GCaMP calcium indicators. Nat Methods *6*, 875-881.

Wallace, D.J., Zum Alten Borgloh, S.M., Astori, S., Yang, Y., Bausen, M., Kügler, S., Palmer, A.E., Tsien, R.Y., Sprengel, R., Kerr, J.N., *et al.* (2008). Single-spike detection in vitro and in vivo with a genetic Ca^{2+} sensor. Nat Methods *5*, 797-804.

Waters, J., Larkum, M., Sakmann, B., and Helmchen, F. (2003). Supralinear Ca^{2+} influx into dendritic tufts of layer 2/3 neocortical pyramidal neurons in vitro and in vivo. J Neurosci *23*, 8558-8567.

Wilt, B.A., Burns, L.D., Wei Ho, E.T., Ghosh, K.K., Mukamel, E.A., and Schnitzer, M.J. (2009). Advances in light microscopy for neuroscience. Annu Rev Neurosci *32*, 435-506.

Zhu, P., Aller, M.I., Baron, U., Cambridge, S., Bausen, M., Herb, J., Sawinski, J., Cetin, A., Osten, P., Nelson, M.L., *et al.* (2007). Silencing and un-silencing of tetracycline-controlled genes in neurons. PLoS ONE *2*, e533.

Auto-luminescent Genetically-Encoded Ratiometric Indicator for Real-time Ca^{2+} Imaging at the Single Cell Level

Kenta Saito[1], Noriyuki Hatsugai[1,2], Kazuki Horikawa[1], Kentaro Kobayashi[1], Toru Matsu-ura[3], Katsuhiko Mikoshiba[3] and Takeharu Nagai[1,4*]

1 Research Institute for Electronic Science, Hokkaido University, Kita-20, Nishi-10 Kita-ku, Sapporo, Hokkaido 001-0020, Japan

2 Research Center for Cooperative Projects, Hokkaido University, Kita-15, Nishi-7 Kita-ku, Sapporo, Hokkaido 060-8638, Japan

3 RIKEN Brain Science Institute, 2-1 Hirosawa, Wako City, Saitama 351-0198, Japan

4 Precursory Research for Embryonic Science, Japan Science and Technology Agency,Sanbancho, Chiyoda-ku, Tokyo 102-0075, Japan

Running title: BRET-based Ca^{2+} indicator

* To whom correspondence should be addressed: tnagai@es.hokudai.ac.jp

Abstract

Background: Efficient bioluminescence resonance energy transfer (BRET) from a bioluminescent protein to a fluorescent protein with high fluorescent quantum yield has been utilized to enhance luminescence intensity, allowing single-cell imaging in near real time without external light illumination.

Methodology/Principal Findings: We applied BRET to develop an autoluminescent Ca^{2+} indicator, BRAC, which is composed of Ca^{2+}-binding protein, calmodulin, and its target peptide, M13, sandwiched between a yellow fluorescent protein variant, Venus, and an enhanced *Renilla* luciferase, RLuc8. Adjusting the relative dipole orientation of the luminescent protein's chromophores improved the dynamic range of BRET signal change in BRAC up to 60%, which is the largest dynamic range among BRET-based indicators reported so far. Using BRAC, we demonstrated successful visualization of Ca^{2+} dynamics at the single-cell level with temporal resolution at 1 Hz. Moreover, BRAC signals were acquired by ratiometric imaging capable of canceling out Ca^{2+}-independent signal drifts due to change in cell shape, focus shift, etc.

Conclusions/Significance: The brightness and large dynamic range of BRAC should facilitate high-sensitive Ca^{2+} imaging not only in single live cells but also in small living subjects.

Introduction

Bioluminescent proteins such as luciferase are a powerful tool for monitoring biological processes including gene expression in living organisms since bioluminescent signals can be acquired without an external light source; bioluminescence imaging is thus completely free from phototoxicity, photo-induced physiological reaction, and autofluorescence from the specimen, enabling signal detection from deep inside the tissue with high signal-to-noise ratio. These properties make bioluminescent proteins potentially superior to fluorescent proteins as a bioimaging tool. However, bioluminescence signals are too dim to be measured in real time, i.e., bioluminescence imaging generally requires longer exposure (more than several tens of seconds) than fluorescence imaging that takes less than 1 second. To overcome this drawback, an auto-illuminating fluorescent protein, eBAF-Y, has been developed [1]. eBAF-Y is based on the highly efficient bioluminescence resonance energy transfer (BRET) between enhanced *Renilla reniformis* luciferase (RLuc8) [2] and enhanced yellow fluorescent protein (EYFP). eBAF-Y emits a 3.5-fold brighter signal than RLuc8 alone, enabling observation of subcellular structure at the single-cell level in near real time at 0.1 Hz. This strategy has been applied to develop a similar auto-illuminating fluorescent protein, BRET3, composed of a mutant red fluorescent protein (mOrange) and RLuc8 [3]. BRET3 exhibits red-shifted light output peaking at 564 nm, making it easier to observe biological phenomena deep inside a small animal. Aequorin, another well-known bioluminescent protein, emits luminescence peaking at 466 nm in the presence of Ca^{2+} so it has been used as a Ca^{2+} indicator to monitor free Ca^{2+} concentration ($[Ca^{2+}]$) in living specimens [4]. The highly efficient BRET has also been applied to aequorin by means of

fusion with green fluorescent protein (GFP), thereby increasing the luminescence intensity by about 50 fold [5]. Although aequorin-GFP is bright enough to allow real-time imaging, it is not suitable for long-term imaging since aequorin must be regenerated after emission upon Ca^{2+} binding, which takes more than several tens of minutes [6,7]. To circumvent this weak point, a Ca^{2+} indicator was developed based on split RLuc and Gluc [8,9]. Signal change of these indicators is based on complementation of the N- and C-terminal halves of the split luciferase via Ca^{2+}-induced interaction between CaM and M13. Although these indicators can detect Ca^{2+}-dependent signal changes in living cells, they could not calibrate $[Ca^{2+}]$ because imaging of these indicators is based on single-emission measurement and thus the signal intensity change is highly dependent on the stoichiometric composition of the N- and C-terminal halves of the split luciferase in the cells. Also, these indicators cannot cancel out signal drift mainly caused by change in cell shape, focus drift, and uptake and consumption of coelenterazine-h due to auto or catalytic oxidization. To allow quantitative long-term real-time Ca^{2+} imaging, we designed a Ca^{2+} indicator based on BRET between RLuc8 and Venus, a brighter version of EYFP [10]. As the Ca^{2+}-sensing domain, we used a Ca^{2+} binding protein, calmodulin (CaM), and its target peptide, M13, as in the case of the well-known FRET-based Ca^{2+} indicator, cameleon [11]. Binding and release of Ca^{2+} from CaM induces reversible conformational change of the CaM-M13 fusion domain between an extended and compact form, which, in turn, changes the distance between Venus and RLuc8 whereby their emission is reciprocally changed due to BRET. Thus, this indicator enables ratiometric observation that can cancel out artifactual signal drift. To obtain a large BRET change, we tried several circularly permuted Venus variants

[12] to optimize the relative dipole orientation between the coelenterazine in RLuc8 and the choromophore of Venus. The best one, which we named BRAC, has a wild-type Venus and showed 60% signal change upon Ca^{2+} binding. Due to the brightness and large dynamic range, we successfully visualized Ca^{2+} oscillation induced by agonist stimulation of Hela cells with improved time resolution and high signal-to-noise ratio.

Results

Construction of BRET-based reversible Ca^{2+} indicators

To create a BRET-based autoluminescent reversible Ca^{2+} indicator, we chose the CaM-M13 chimeric protein for the Ca^{2+}-sensing domain as in the case of the FRET-based Ca^{2+} indicator, cameleon YC3.60 (see Ref. 12). ECFP in YC3.60 was first replaced with RLuc8, the brightest version of luciferase [2], to yield RLuc8-CaM-M13-cp173Venus (Figure 1). The construct was bacterially expressed and purified for measuring the signal change in the peak intensity ratio (530/480 nm) with Ca^{2+}. The dynamic range of the BRET signal change in RLuc8-CaM-M13-cp173Venus was 10% (Figure 2). Then, according to the strategy for expanding the dynamic range of FRET-based indicators [12], we replaced the Venus moiety in RLuc8-CaM-M13-Venus with a wild-type Venus or circularly permuted Venus variants that have a different translation start site from the original cp173Venus, as shown in Figure 1A. Among them, RLuc8-CaM-M13-Venus and RLuc8-CaM-M13-cp157Venus showed a 3-fold enhanced dynamic range (Figure 2). To further expand the dynamic range, we attempted to exchange the donor and acceptor in the above constructs to place the donor and acceptor molecule at the C- and N-terminus,

respectively, of CaM-M13 (Figure 1A). Of these constructs, Venus-CaM-M13-RLuc8 had a 2-fold higher dynamic range than RLuc8-CaM-M13-Venus and RLuc8-CaM-M13-cp157Venus while other constructs showed a lower dynamic rang (Figure 2)e. This result was consistent with previous results showing that orientation in which the donor luciferase was located at the C-terminus of the fusion generated a higher BRET signal compared to the reverse orientation [1,13]. Overall, Venus-CaM-M13-RLuc8, which we designated as BRAC (BRet-based Autoluminescent Ca^{2+} indicator), had the largest dynamic range (60%) among the constructs that we tested (Table 1).

Physicochemical properties of BRAC

To evaluate the chemical properties of BRAC, Ca^{2+} titration was carried out. As shown in Figure 3A, emission from acceptor Venus increased in accordance with [Ca^{2+}] while emission from donor RLuc8 was almost constant. This result closely corresponds to the result from the BRET-induced luminescence enhancement in BAF-Y as reported previously[1]. Ca^{2+} titration revealed that BRAC gave a monophasic Ca^{2+} response curve with a Hill coefficient of 1.3, and apparent dissociation constant of 1.9 μM (Figure 3B). We also perform pH titration of BRAC, which indicated that the emission ratio of 530 to 480 nm in BRAC was stable in physiological pH between 6.5 and 8.0 (Figure 3C). We then measured the Ca^{2+}-association kinetics of BRAC by stopped-flow photometry system. However, the time course data we obtained was composed of at least two exponential decay components ($\tau < 0.1$ sec) which were thought to be derived from both Ca^{2+} and coelenterazine-h binding to BRAC. Because both kinetics were quite similar, we could not

distinguish which component was derived from Ca^{2+} binding to BRAC. Thus, we then measured Ca^{2+}-dissociation kinetics of BRAC (Figure 3D). The dissociation time constant of BRAC (τ=0.21 sec) was independent on Ca^{2+} concentration and much smaller than that of YC3.60 (τ=2.9 sec, k_{off}=0.34 s^{-1}) (Figure 3E, F) and comparable to that of G-CaMP (τ=0.19 sec) [14]. This result was in good agreement with the fact that Ca^{2+} affinity of BRAC (K_d = 1.9 μM) is about 10 times lower than that of YC3.60 (K_d = 0.25 μM), and indicated that association/dissociation kinetics of BRAC are fast enough to detect Ca^{2+} dynamics in living cells and organelles.

Ca^{2+} imaging by BRAC in living Hela cells

In order to determine the validity of BRAC in living cells, we transfected Hela cells with the cDNA encoding BRAC. Direct excitation of the Venus moiety with blue light revealed that BRAC was localized in the cytoplasmic compartment, and slightly in the nucleus (Figure 4A). Figure 4B, 4C and 4D show the time course of RLuc8 and Venus, and pseudo-colored Venus/RLuc8 ratio images, respectively (see Supporting Video 1). Upon stimulation with 10 μM histamine, RLuc8 signals did not show a spike-like shape and sometimes increased or decreased slightly while Venus signals showed an oscillated spike after histamine stimulation as well as drifting of basal signal intensity, as seen in RLuc8 signals (Figure. 4E). The drift observed in both RLuc8 and Venus signals might be caused by the uptake and consumption of coelenterazine-h or the change in cell shape. However, due to the ratiometric imaging of BRAC, this signal drift was successfully canceled out by dividing the Venus signal with that of RLuc8 (Figure 4F). We also examined the dynamic

range of BRAC in Hela cells by measuring minimum and maximum BRET ratio values which were obtained by treatment of HeLa cells with ionomycin/1mM EGTA and ionomycin/5mM $CaCl_2$, respectively. The dynamic range obtained was 44% which was comparable to that measured *in vitro*.

For further validation of BRAC as an auto-luminescent Ca^{2+} indicator, we compared performance of BRAC with other BRET-based Ca^{2+} indicator, G5A [5] in HeLa cells. The signal to noise ratio of G5A was much better than that of BRAC (Figure 4G) because G5A did not emit any luminescence before Ca^{2+} binding. However, G5A failed to report histamine-induced Ca^{2+} oscillations that were reproducibly observed by using BRAC (Figure 4F, 4G), probably due to much slow regeneration rate of aequorin from apoaequorin [6,7]. This result indicates the superiority of BRAC in terms of long term imaging of Ca^{2+} dynamics.

Ca^{2+} imaging by BRAC in plant tissue

To further examine BRAC performance, we tried Ca^{2+} imaging in plant leaves, in which fluorescence-based Ca^{2+} imaging is difficult owing to the chloroplasts-derived strong auto-fluorescence, which disturbs reliable detection of fluorescence signal from Ca^{2+} indicator. Ca^{2+} is a ubiquitous intracellular second messenger involved in numerous signaling pathways in plants. Elevation of cytosolic Ca^{2+} concentration ($[Ca^{2+}]_i$) are common early event in plant defense signaling, and Ca^{2+} plays a essential role in activating the plant's surveillance system against attempted microbial invasion [15]. *Arabidopsis thaliana* has resistance to *Pseudomonas syringae* pv. *Tomato* (*Pst*) DC3000 having the